Level density and mechanism of deuteron-induced reactions on ^{54,56,58}Fe

A. P. D. Ramirez, A. V. Voinov, S. M. Grimes, Y. Byun, C. R. Brune, T. N. Massey, S. Akhtar, S. Dhakal, and C. E. Parker

Phys. Rev. C **92**, 014303 — Published 6 July 2015

DOI: 10.1103/PhysRevC.92.014303

Level density and mechanism of deuteron-induced reactions on ^{54,56,58}Fe

A. P. D. Ramirez,* A. V. Voinov, S. M. Grimes, Y. Byun,
C. R. Brune, T. N. Massey, S. Akhtar, S. Dhakal, and C. E. Parker
Department of Physics and Astronomy, Ohio University, Athens OH, 45701, USA

Deuteron elastic cross sections, as well as neutron, proton, and α-particle emission spectra, from d + ^{54,56,58}Fe reactions have been measured with deuteron beam energies of 5, 7, and 9 MeV. Optical model parameters have been tested against our experimental data. The fraction of total reaction cross section responsible for the formation of compound nuclei has been deduced from the angular distributions. The degree of discrepancy between calculated and experimental compound cross sections was found to increase with increasing neutron number. The nuclear level densities of the residual nuclei ^{55}Co, ^{57}Co, ^{55}Fe, ^{57}Fe, ^{52}Mn, and ^{54}Mn have been deduced from the compound double differential cross sections. The Gilbert-Cameron model with Iljinov parameter systematics [1] was found to have a good agreement with our results.

I. I. INTRODUCTION

The knowledge of nuclear reaction cross sections is crucial in many nuclear physics applications. For example, extensive cross-section data are essential to carry out a complete astrophysical network calculation for the s-, r-, and p-processes nucleosynthesis or to design the future fusion reactors. Hence, an accurate theoretical prediction of cross sections is important, especially in cases where experimental data are scarce or unavailable. At low bombarding energies, the compound nuclear reaction is known to be the dominant mechanism. For reactions that involve medium and heavy mass nuclei, which exhibit high density of excited states, the compound cross section is calculated using the framework of the statistical Hauser-Feshbach (HF) theory [2]. The HF theory uses the transmission coefficients and nuclear level densities as its input parameters. For a reaction $A(a,b)B$, the compound cross section is expressed as follows:

$$\sigma_{ab}(\varepsilon_a,\varepsilon_b) = \sum_{J,\pi} \sigma^{CN}_{J,\pi}(\varepsilon_a) \frac{T_b(\varepsilon_b)\cdot\rho_b(E^*_b)}{\sum_c \int_{\varepsilon_c} T_c(\varepsilon_c)\cdot\rho_c(E^*_c)d\varepsilon_c}. \quad (1)$$

Here, ε_a and ε_b are the energies of the incoming and outgoing channels, respectively, $\sigma^{CN}_{J,\pi}$ is the cross section for the formation of the compound nucleus in state J and parity π, T_b is the transmission coefficient of the emitted particle b, and $\rho_b(E^*_b)$ is the level density of the residual nucleus B at an excitation energy E^*_b. The denominator on the right hand side of equation (1) represents the sum over all possible reaction channels c. The level densities and transmission coefficients for the outgoing channels imply summation over spins and parities, which is omitted for simplicity in the equation. Among the input parameters, the level density has often been considered to contribute the largest uncertainty in the calculated cross section.

A common practice in using the HF theory is to assume a model function that predicts the nuclear level density over the required range of excitation energies. There are several phenomenological models available for this purpose. Most of them are based on the Fermi gas model [3] given by

$$\rho(E) = \frac{\exp\left[2\sqrt{a(E-\delta)}\right]}{12\sqrt{2}\sigma a^{1/4}(E-\delta)^{5/4}}, \quad (2)$$

where σ is the spin cut-off parameter that describes the width of the spin distribution function, δ is the pairing energy that accounts for the even-odd differences in the nuclear binding energy, and a is the level density parameter that is related to the density of single particle states near the Fermi energy. Both the level density parameter a and the spin cut-off parameter σ in equation (2) are also assumed to be model functions. An extensive choice of models is already a concern for an accurate level density prediction. In addition, each model has several options for level density parameters.

The level density model parametrization is traditionally based on counting both the discrete levels near the ground state and the neutron resonances around the neutron binding energy. The density of discrete levels and the average neutron resonance spacings are generally well documented in the literature [4, 5], although some discrepancy between data from Refs. [4] and [5] exists. The level density in the energy interval between discrete levels and neutron resonances remains largely uncovered by experiment. The neutron resonance data, however, provide level density information in very narrow range of excitation energies and spins. Moreover, there is an uncertainty in the assumed spin and parity distributions because of the lack of experimental data in this energy region. These factors could result in the uncertainty of the deduced level density for other spins. Therefore, it is important to use a different technique for acquiring the experimental level density that would cover wider excitation energy, spin, and parity ranges.

In this paper, we study the level densities of ^{55}Co, ^{57}Co, ^{55}Fe, ^{57}Fe, ^{52}Mn, and ^{54}Mn from the particle evaporation spectra of d + ^{54,56}Fe reactions. The particle emission spectra from compound nuclear reactions have

* ar765608@ohio.edu

been shown to provide level density information for excitation energies from near the ground state up to the particle separation energy [6]. To minimize the contribution from non-compound mechanisms, it is important to use appropriate reactions and projectile energies. The applicability of deuteron-induced reactions to study level density has been explored in Ref. [7] on ^{59}Co. Here, we used deuterons on ^{54,56,58}Fe to see how the reaction mechanisms and the level densities of the above mentioned nuclei depend on the N/Z ratio of iron isotopes. The deuteron elastic scattering was also measured to find the best optical model parameters to estimate the total reaction cross sections.

II. II. EXPERIMENT

The experiments were carried out at the Edwards Accelerator Laboratory of Ohio University using the 4.5-MV tandem accelerator. Pulsed deuteron beams, with energies of 5, 7, and 9 MeV, were incident on ^{54}Fe, ^{56}Fe, and ^{58}Fe self-supporting foils with thicknesses (isotopic abundances) 610 μg/cm^2 (>95%), 538 μg/cm^2 (>95%), and 647 μg/cm^2 (81 %), respectively. The typical deuteron beam intensities were 65 nA and 200 nA for the charged particle and neutron measurements, respectively. Each target foil was bombarded with deuteron beam for a duration of 1.5 - 2 hours. The emitted neutrons and charged particles, including protons, deuterons, and α particles, were measured in forward and backward angles. The typical rates at backward angles with E$_d$ = 7 MeV were 17 counts/s, 5 counts/s, 1.5 counts/s, and 55 counts/s for (d,p), (d,d), (d,α), and (d,n) channels, respectively.

Neutron emission spectra were measured at angles between 20° and 150° with the swinger facility. The swinger beam line has a unique capability of bending the accelerated beam perpendicular to its original direction. To study neutron angular distributions, the swinger beam line rotates along the original axis of the beam while the detectors are placed at a fixed location. A detailed description of the beam swinger facility is given in Ref. [8].

In our experiment, the NE213 scintillation neutron detector coupled to a photomultiplier tube (PMT) was positioned in the time-of-flight (TOF) tunnel at a distance of about 7 m from the target position. The detector efficiency was measured using the ^{27}Al(d,n) reaction at a deuteron energy of 7.44 MeV and an emission angle of 120° [9]. The absolute efficiency was found to be about 30% for 2 MeV neutrons, and it gradually decreased to 20% as the neutron energy increased to 14 MeV. These numbers do not include the solid angle covered by the detector. The pulse shape discrimination technique was employed to separate the events generated by neutrons and γ rays. The neutron energy spectra were then obtained by the time-of-flight method. We also acquired the target-out spectra to account for background.

Charged particle measurements were performed using the charged particle spectrometer composed of a target chamber with attached TOF tubes and silicon surface barrier detectors as shown in Figure 1. The detectors were positioned such that they cover the angular range from 37.5° to 157.5°. The flight path in the forward directions was about 2 m, whereas in the backward directions, it was about 1.5 m. The energy calibration of the silicon detectors was done using deuterons and protons that populate the discrete levels in ^{12}C(d,p)^{13}C, ^{197}Au(d,d)^{197}Au, and ^{54}Fe(d,p)^{55}Fe reactions. For the particle identification, we simultaneously acquired the energy deposited in the detector and the flight time to separate registered events according to the mass of the charged particles. For deuterons, only the elastic peak had good statistics. The cross sections for deuterons, tritons, and ^{3}He at lower outgoing energies were too small to be measured accurately.

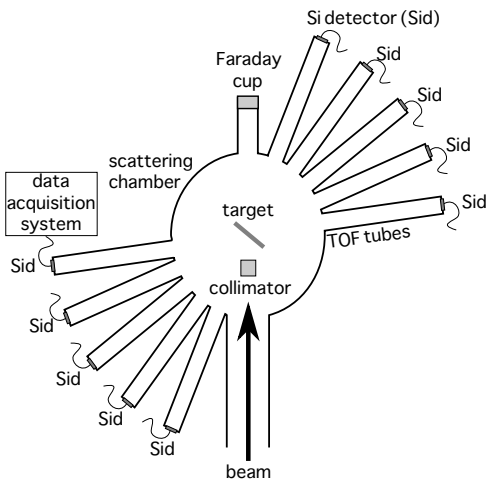

FIG. 1. Schematic of the charged particle spectrometer.

III. III. ELASTIC SCATTERING MEASUREMENTS

The optical model potential (OMP) is often applied in calculations to provide transmission coefficients and total reaction cross sections. In the HF model, the total reaction cross section is assumed to be equal to the compound nucleus formation cross section σ^{CN}. If non-compound mechanisms are involved, the compound cross section would represent a fraction of the total cross section estimated from optical model potentials. In this case, a constant multiplication factor needs to be used to account for the non-compound component due to direct and pre-equilibrium processes.

Recent studies [10, 11] have shown that measured differential elastic scattering cross sections of deuterons on medium-mass nuclei were not reproduced by theoretical calculations, especially at backward angles and for bombarding energies below 20 MeV. Using our elastic scatter-

ing data, we examined known optical model parameters for deuteron energies below 10 MeV. Here, we considered the optical model parameter sets from Lohr et al. [12], Bojowald et al. [13], and Haixia et al. [14] It is important to note that the Bojowald and Lohr parameters are recommended only for deuteron energies above 20 and 8 MeV, respectively. Therefore, they have been extrapolated down to 5 MeV for further analysis. The OMP parameters were retrieved from the Reference Input Parameters Library (RIPL-3) [4].

Figure 2 shows the comparison of our experimental data points and theoretical calculations for the ratio of elastic scattering to Rutherford cross sections for ^{54}Fe(d,d)^{54}Fe, ^{56}Fe(d,d)^{56}Fe, and ^{58}Fe(d,d)^{58}Fe reactions at bombarding energies of 5, 7, and 9 MeV. There is a relatively good agreement between predictions from different parameter sets and the present data for angles below 50°, which is attributed to the strong influence of Coulomb scattering. It is in the backward angles where we see divergence in the predictions. In Figure 2(d) and 2(e), the elastic scattering data points for 5- and 7-MeV deuterons on ^{56}Fe by Al-Quraishi et al. [15] are also plotted. Their data are in very good agreement with our experimental points.

The Lohr parametrization is consistently in better agreement with our elastic scattering experimental data for all bombarding energies. Therefore, we utilized this parametrization to describe the optical parameters of the entrance channel in our HF analysis. The calculated absorption cross sections according to the OMP parameter sets considered in this study are tabulated in Table I. The absorption cross sections for the d + ^{56}Fe reaction can be compared with the optimum values acquired by Ref. [15] since they have performed a best-fit procedure on their elastic scattering data. They arrived at the values of 561 mb and 1074 mb for deuteron energies of 5 and 7 MeV, respectively, which are close to the values from Lohr as listed in Table I. From the table, it is also apparent that the calculated cross sections based on the Haixia parametrization are very similar with those from Lohr.

Nucleus	Energy (MeV)	Haixia [14] (mb)	Lohr [12] (mb)	Bojowald [13] (mb)
^{54}Fe	5	536	542	617
	7	985	994	1093
	9	1244	1260	1368
^{56}Fe	5	553	558	636
	7	1008	1015	1117
	9	1270	1282	1395
^{58}Fe	5	571	573	655
	7	1031	1034	1142
	9	1296	1303	1421

TABLE I. Deuteron absorption cross sections as predicted by different optical model potentials.

For the transmission coefficients of the outgoing neutrons and protons, we employed the OMP parameters of

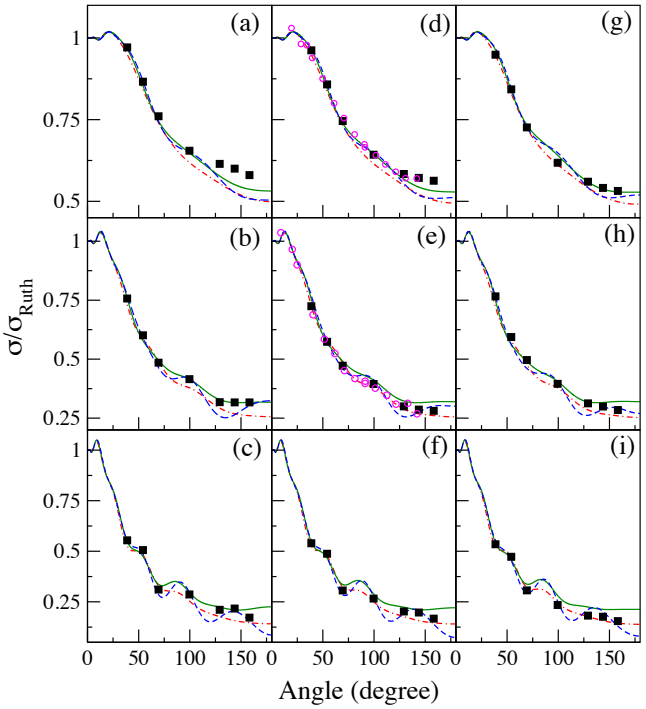

FIG. 2. (Color online) Ratio of deuteron elastic scattering to Rutherford cross sections in the center-of-mass system for: ^{54}Fe(d,d)^{54}Fe with E_d = 5 MeV (a), E_d = 7 MeV (b), and E_d = 9 MeV (c); ^{56}Fe(d,d)^{56}Fe with E_d = 5 MeV (d), E_d = 7 MeV (e), and E_d = 9 MeV (f); ^{58}Fe(d,d)^{58}Fe with E_d = 5 MeV (g), E_d = 7 MeV (h), and E_d = 9 MeV (i). Lines are theoretical calculations from optical parameters of Bojowald et al. [13] (dashed-dotted), Lohr et al. [12] (solid line), and Haixia et al. [14] (dashed) while points are experimental data from this work (solid square) and from Al-Quraishi et al. [15] (open circle).

Koning et al. from Ref. [16], whereas the OMP parameters of McFadden et al. from Ref. [17] were utilized for the transmission coefficients of the outgoing α particles.

IV. IV. CROSS SECTIONS AND ANGULAR DISTRIBUTIONS

The absolute double differential cross section in the laboratory frame of reference is determined from the measured particle spectrum, the target thickness, the detector efficiency, the integrated charge of the incident beam, and the solid angle subtended by the detector. The cross sections are further transformed to the center-of-mass system (CM) in order to compare them with theoretical calculations. Special care was taken in obtaining the cross sections from the d + ^{58}Fe reaction since the target contained only about 81% of the ^{58}Fe isotope. Proton peaks related to ^{56}Fe(d,p) reaction have been identified in the ^{58}Fe(d,p) spectrum. Based on the integrated counts of those peaks, the ^{56}Fe(d,p) spectrum was renormalized and subtracted to reactions from the ^{58}Fe(d,p) spectrum.

No proton peaks related reactions on other iron isotopes have been located in the ^{58}Fe(d,p) spectrum.

When using an evaporation spectrum to study the nuclear level density, it is important that the experimental cross section has negligible contamination from non-compound reactions. This is inferred by analyzing the angular distribution of emitted particles. The outgoing particles from compound nuclei decay are expected to have a symmetric angular distribution about 90° in the CM system. On the other hand, non-compound contributions due to direct and pre-equilibrium emissions have an asymmetric distribution favoring the forward direction. A previous study [7] has indicated that particle spectra measured at backward angles from deuteron-induced reactions on cobalt are dominated by compound emissions. Based on this finding and taking into account the fact that the angular distributions are flat at backward angles, we assume that the direct processes (including deuteron break-up mechanism) have negligible contribution to the particle spectra measured at backward angles. For purely compound nuclear reactions, studying the angular distribution is also an essential tool to extract information of the spin cut-off parameter in the spin distribution function [18].

Figure 3 shows the angular distributions of emitted protons and α particles for selected energy intervals. The angular distributions exhibit an asymmetry with a prominent forward-peaked component attributed to non-compound reaction mechanisms. The forward angle anisotropy is more pronounced for protons. The backward angles display a flattening of the angular distributions. Such a pattern indicates the dominance of compound emissions at backward angles. Further inspection reveals that proton angular distributions appear to be more forward peaked for higher proton energies. This suggests that non-equilibrium processes, particularly direct reactions, play a larger role in these proton emissions and may likely contribute to the spectra even at backward angles, especially for very high proton energies.

Since we did not perform the ^{56}Fe(d,n) reaction, we adopted the cross sections from Ref. [15] for the same reaction with a bombarding energy of 7 MeV. It stated that the angular distribution of the neutron spectra is almost flat for angles beyond 80°. The same angular distribution is seen in our data for the ^{54}Fe(d,n) and ^{58}Fe(d,n) reactions.

In order to estimate the compound fraction of the total cross section, we separated the symmetric (compound) and forward-peaked (non-compound) components of the angular distribution using the phenomenological Kalbach formula (see equation (3) of Ref. [19]). As mentioned in section III, this is essential to correct theoretical calculations for the incident flux that proceeds through non-compound reactions. For data with E_d = 7 MeV, we estimated the compound fractions obtained from neutron, proton, and α-particle angular distributions, while for data with E_d = 5 and 9 MeV, the fractions were estimated only from proton and α-particle emission data.

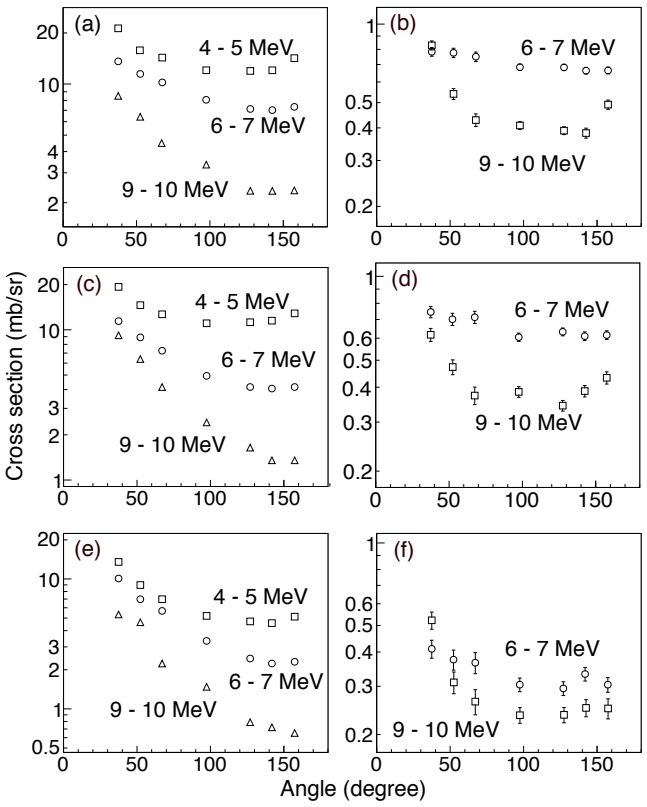

FIG. 3. Angular distributions in the CM system from ^{54}Fe(d,p) (a), ^{54}Fe(d,α) (b), ^{56}Fe(d,p) (c), ^{56}Fe(d,α) (d), ^{58}Fe(d,p) (e), and ^{58}Fe(d,α) (f) emission spectra integrated over selected energy intervals for deuteron energy of 9 MeV.

Table II summarizes the estimated compound fractions of the total reaction cross sections from d + ^{54,56,58}Fe reactions. Similar tabulations were reported for d + ^{56}Fe reaction by Mishra et al. [20] (from neutron measurements only) and Al-Quraishi et al. [15]. The decreasing pattern of our compound fractions with respect to bombarding energy is supported by the results from Al-Quraishi, while the results from Mishra indicated an increasing trend. The decreasing trend for deuteron energies greater than 5 MeV on ^{54,56}Fe isotopes has also been shown in the theoretical estimations of Ref. [11] while for ^{58}Fe they indicated an increasing trend up to about 9 MeV of the deuteron energy. The reason for the discrepancy is not clear at the moment. This ambiguity needs to be resolved in future experiments.

	d + ^{54}Fe	d + ^{56}Fe	d + ^{58}Fe
E_d (MeV)	Compound fraction(%)		
5	84	76	73
7	72	65	64
9	68	57	39

TABLE II. Estimate of compound fractions obtained from the analysis of angular distributions.

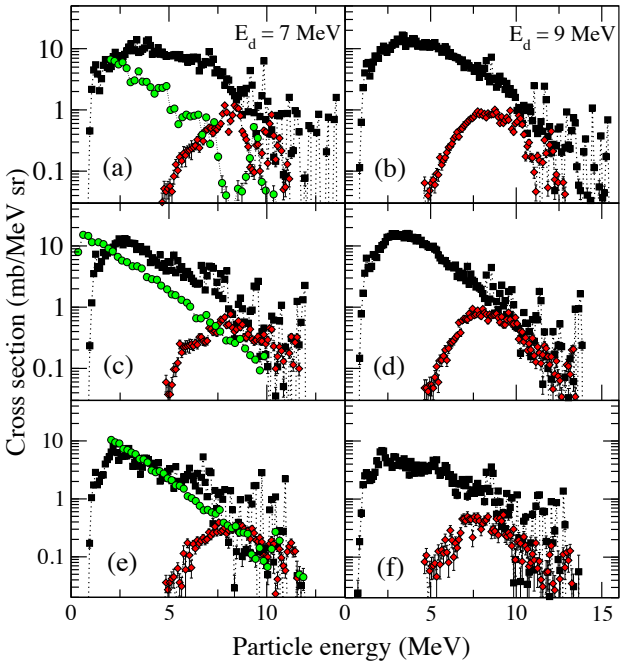

FIG. 4. (Color online) Neutron (circle), proton (square), and α particle (diamond) cross sections measured at backward angles from d + ^{54}Fe reaction with E_d = 7 (a) and 9 MeV (b), d + ^{56}Fe reaction with E_d = 7 (c) and 9 MeV (d), and d + ^{58}Fe reaction with E_d = 7 (e) and 9 MeV (f).

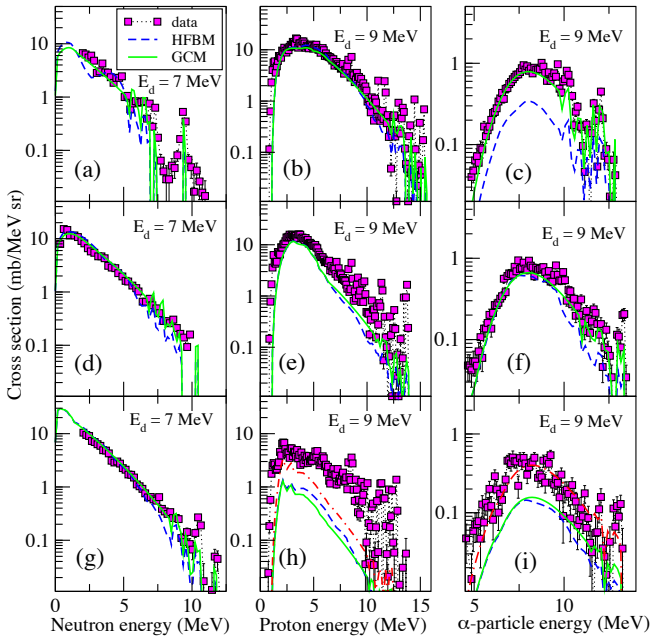

FIG. 5. (Color online) Comparison of experimental and theoretical calculations of differential cross sections for ^{54}Fe(d,n) (a), ^{54}Fe(d,p) (b), ^{54}Fe(d,α) (c), ^{56}Fe(d,n) (d), ^{56}Fe(d,p) (e), ^{56}Fe(d,α) (f), ^{58}Fe(d,n) (g), ^{58}Fe(d,p) (h), and ^{58}Fe(d,α) (i) reactions measured at backward angles. Lines are theoretical calculations. Dashed-dotted line (red) is calculation using the GCM without the correction from compound fraction.

Figure 4 shows the neutron, proton, and α-particle spectra in the CM system from d + ^{54,56,58}Fe reactions measured at 142.5°. The error bars presented in the figure are due to counting statistics only. A systematic uncertainty of about 22% should be added for the total uncertainty. This includes a 15% uncertainty for the transmission coefficient, which arises from different systematics of optical model parameters, and about 15% uncertainty of the target thickness. In Figure 4(a), clear irregularities of the ^{54}Fe(d,n) cross sections are observed, particularly in the neutron energy region between 5 and 7.5 MeV. Inspection of the target-in and target-out TOF spectra for this reaction revealed contamination from d + ^{12}C reaction. Therefore, we emphasized more on energies below 5 MeV to compare with theoretical calculations. It can also be seen in Figures 4(a), 4(c), and 4(e) that the ratio of neutron to proton emission cross sections for E_d = 7 MeV increases with isotopic number of the target nuclei. The preference of neutron emission over proton emission for high isotopic number is clearly due to the decrease in neutron separation energy and the increase in proton separation energy. For the purpose of level density study, we utilized the neutron cross sections obtained with E_d = 7 MeV and the proton and α-particle cross sections with E_d = 9 MeV.

For theoretical calculations, we used the nuclear reaction code EMPIRE [21]. Here, we tested the following level density models available in EMPIRE: the Gilbert-Cameron model (GCM) [22] using the Iljinov level density parameter systematics [1]; and the microscopic model using the combinatorial approach on the single particle levels obtained from the Hartree-Fock-Bogoliubov method (HFBM) [23]. We also tested the Fermi gas model (FGM) (2) using the von Egidy parameter systematics [24].

The Gilbert-Cameron model [22] is a combination of two model functions. The lower excitation energy region is described by the constant temperature model (CTM) [25] such that

$$\rho_{CT} = \frac{1}{T}\exp\left(\frac{E-E_0}{T}\right), \qquad (3)$$

where T is the nuclear temperature and E_0 is the energy shift, while the higher excitation energy region follows the Fermi gas model function (2). In addition to the free parameters in both model functions, a matching energy E_M is also defined such that both level densities and their derivative are continuous at this point.

In the Gilbert-Cameron approach, the Fermi gas model component is employed with an energy-dependent level density parameter a according to Ref. [26] to account for the shell effects. This is expressed as

$$a(U) = \tilde{a}\left[1+\delta W\frac{\exp(\gamma U)}{U}\right], \qquad (4)$$

where $\tilde{a}$ is the asymptotic level density parameter, δW is the shell correction energy, γ is the damping parameter,

and U is the "effective" excitation energy, such that $U = E - \delta$. The spin cut-off parameter in equation (2) follows the expression

$$\sigma^2 = 0.1461 A^{2/3} \sqrt{aU}, \quad (5)$$

where A is the nuclear mass number. It should be noted though that the Iljinov systematics for GCM provide the asymptotic level density parameter $\tilde{a}$ and the damping parameter γ. The values of temperature T and energy shift E_0 result from fitting the discrete levels in the low-excitation energy region and the FGM level density at the matching point E_M.

The comparison between experimental differential cross sections and theoretical calculations is shown in Figure 5. The predictions according to the Gilbert-Cameron model (GCM) describe the shape of all the experimental cross sections well. However, there is a growing discrepancy in the cross section magnitude as the neutron number of the iron isotope increases. There is a good consistency for ^{54}Fe, a slight underestimation of experimental protons and α-particles by calculations for ^{56}Fe, and a large underestimation observed for ^{58}Fe(d,p) and ^{58}Fe(d,α). The reason for such a tendency is not yet clear. To exclude any uncertainties in the calculations caused by the correction on compound fraction, we performed calculations of ^{58}Fe(d, p) without compound fraction correction (see Figure 5). The prediction still underestimates the experimental proton cross sections by almost a factor of 2. One can speculate that there is some multistep compound process, which results in an almost symmetric angular distribution, but the compound nucleus has not yet totally equilibrated when the proton or α-particle emission occurs. Such a process can increase the cross section of outgoing particles. To verify such a hypothesis, the proton and α-particle emission cross sections need to be measured with different entrance channel reactions that excite the same compound nucleus. It is also possible that a compound nuclear process occurs as the second stage of a reaction where the first step is direct or pre-equilibrium. Our calculations are based on the assumption that compound reactions occur starting from the first compound nucleus (one formed by a deuteron combining with a target nucleus). A proton, for example, could be emitted from the compound nucleus formed by the capture of a proton released from a deuteron break-up.

We found that the GCM model with Iljinov systematics best describes our experimental data. Parameters that were used to calculate the GCM level density are tabulated in Table III. For HFBM, in most cases, the slope is slightly steeper than from the experiment. It also predicts an oscillation in the cross section for the ^{54}Fe(d, n) reaction, as shown in Figure 5(a), which is not observed in our data. Moreover, we found a significant difference in the magnitude of the cross section for the ^{54}Fe(d,α) reaction, as displayed in Figure 5(c).

V. V. NUCLEAR LEVEL DENSITIES

The experimental nuclear level density is extracted from experimental particle evaporation spectra using the Hauser-Feshbach model given in equation (1). The main idea is to optimize the parameters of the input level density model $\rho_{\rm mod}$ such that the calculated double differential cross section $\frac{d\sigma}{dE}|_{\rm mod}$ reproduces the experimental data $\frac{d\sigma}{dE}|_{\rm exp}$ as close as possible. The next step is to perform binwise renormalization procedure according to the expression

$$\rho_{\rm expt} = \rho_{\rm mod} \frac{\frac{d\sigma}{dE}|_{\rm exp}}{\frac{d\sigma}{dE}|_{\rm mod}}, \quad (6)$$

as suggested by Vonach in Ref. [6].

Since the absolute level densities after such a renormalization are still uncertain, the absolute normalization is done by matching the experimental data points $\frac{d\sigma}{dE}|_{\rm exp}$ to the calculated ones $\frac{d\sigma}{dE}|_{\rm mod}$ in the region of known discrete low-lying levels. In some of the nuclei, however, experimental data points are not available in the high energy region corresponding to population of discrete levels due to contamination from non-compound emissions. In such a case, we make an absolute normalization of the final $\rho_{\rm expt}$ to ensure that it reproduces the density in the discrete level region by utilizing model extrapolation. The uncertainty in the normalization procedure is up to a factor of 2, which is due to the uncertainty in the types of extrapolation function and not accounting for the level density structure at low excitation energies. Here, as an extrapolation function, we used the constant temperature formula given in equation (3). This procedure was carried out for the residual nuclei populated by (d,p) reactions.

Figure 6 presents the experimental level densities of the residual nuclei ^{55}Co, ^{55}Fe, and ^{52}Mn populated by neutron, proton and α-particles from d + ^{54}Fe; and ^{57}Co, ^{57}Fe, and ^{54}Mn from d + ^{56}Fe reactions, respectively. We have also included the results obtained by other authors for the same nuclei but using different reactions. Our level density function for ^{57}Co is in reasonable agreement with the one obtained by Mishra et al. from the ^{57}Fe(p, n) reaction [20]. The level density of the ^{54}Mn nucleus obtained by Zhuralev et al. [27] is consistent with the general slope of our data, but it is higher in absolute magnitude. This might manifest difficulties with the absolute normalization procedure. We also noticed a structure in the Zhuralev data that is consistent with our results such as the one around 4 MeV (see Figure 6(f)), but not for the bump located at 2.5 MeV. For the ^{57}Fe nucleus, our data points are not consistent in absolute numbers with the results from Voinov et al. [7] (given by red points) and from Schiller et al. [28] (given by blue points). Again, the difference in magnitude can be explained by different normalization procedure used in different types of reactions. In our case, since the constant temperature model used for extrapolation varies

Nucleus	GCM (Iljinov sys) [1]					Experiment (best-fit)	
	$\tilde{a}$	δ	E_M	E_0	T	T	E_0
	(MeV^{-1})	(MeV)	(MeV)	(MeV)	(MeV)	(MeV)	(MeV)
^{55}Co	7.69	1.62	7.22	-0.46	1.35	1.44 (0.26)	-0.95 (1.65)
^{55}Fe	7.11	1.62	9.51	-1.75	1.49	1.47 (0.15)	-1.70 (1.20)
^{52}Mn	7.30	0	5.99	-1.53	1.23	1.30 (0.14)	-1.81 (0.90)
^{57}Co	7.95	1.59	8.86	-1.60	1.36	1.41 (0.06)	-1.91 (0.45)
^{57}Fe	7.64	1.59	9.87	-2.26	1.39	1.44 (0.05)	-2.62 (0.40)
^{54}Mn	7.55	0.0	7.48	-2.40	1.29	1.29 (0.07)	-2.50 (0.50)
^{59}Co	9.30	1.56	6.92	-0.89	1.07		
^{56}Mn	8.82	0.0	7.08	-2.52	1.10		

TABLE III. GCM parameters from Iljinov level density parameter systematics. Best-fit parameters for constant temperature model are also shown. Value in parenthesis is the uncertainty of the parameter.

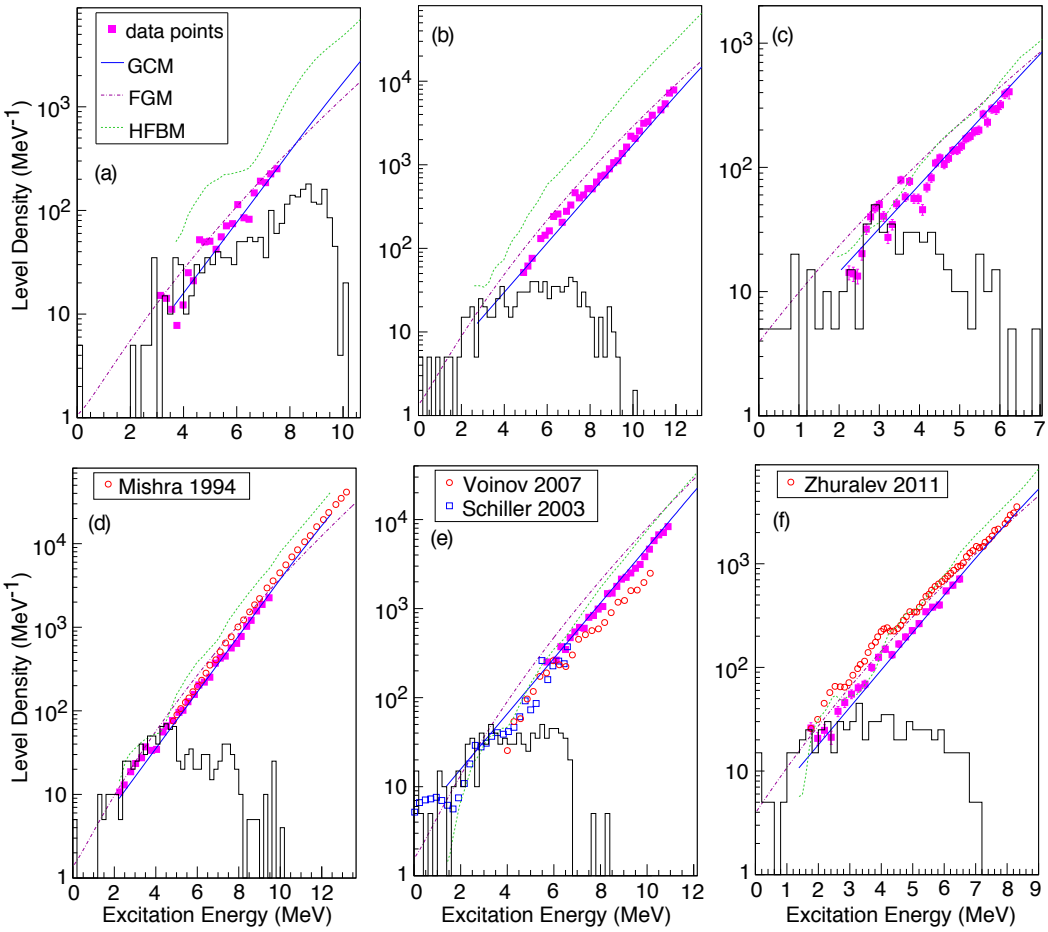

FIG. 6. (Color online) Level densities of ^{55}Co (a), ^{55}Fe (b), ^{52}Mn (c), ^{57}Co (d), ^{57}Fe (e), and ^{54}Mn (f) nuclei. Solid points are present experimental values; open points are data from (Mishra 1994: [20]), (Voinov 2007: [7]), (Schiller 2003: [28]), and (Zhuralev 2011: [27]); histograms are density of low-lying discrete levels; and lines are calculations from Gilbert-Cameron model (solid), Fermi gas model (dashed-dotted), and microscopic model (dashed).

smoothly with excitation energy, it is not capable of reproducing the structures in the level density that may be associated with inherent properties of the nucleus being studied. As an example, the step structure at about 3 MeV (as shown in Figure 6(e)), which appears in the data points reported by Schiller, is believed to be due to the breaking of a nucleon Cooper pair.

We also compared our experimental level densities with known models as shown in Figure 6. The calculated level densities based on the Gilbert-Cameron model (GCM) with parameter systematics according to Iljinov [1] consistently describes our results well for all nuclei. This is

also shown in Table III as we compare our best-fit parameters with the predictions from the Iljinov systematics. As listed, a very close agreement with the parameters of the constant temperature model, particularly for the temperature T, is found. Since the average matching energy E_M, where CTM transitions to FGM, for all nuclei is about 7.5 MeV, the FGM component of the Gilbert-Cameron model has almost negligible influence on the predicted level densities. On the other hand, the calculated level densities based on the microscopic HFBM model describe the slopes of our experimental level densities reasonably well, but they consistently overestimate the absolute magnitude. Similarly, the level densities based on the FGM with parameter systematics according to von Egidy [24] resemble the slopes for most of our data, but they slightly overestimate the magnitude for some of the nuclei.

A close examination of the experimental data points and calculations presented in Figure 6 shows the tendency of the experimental level densities to favor the constant temperature model rather than the Fermi gas model in the whole excitation energy range. This justifies using the CT model in the extrapolation procedure for the normalization of the data. This observation is in line with other similar level density measurements obtained from different experiments and in different mass ranges [29, 30]. The growing number of experimental evidences supporting the constant temperature model might indicate its common physics origin, which needs to be understood.

VI. VI. SUMMARY AND CONCLUSION

The neutron, proton, and α-particle emission spectra from d + ^{54,56,58}Fe reactions have been measured, and differential cross sections have been obtained. Optical model parameters have been tested against experimental ^{54,56,58}Fe(d,d) elastic scattering cross sections. Analysis of the angular distributions of reaction products indicates the presence of compound and non-compound emissions. However, the cross sections measured at backward angles are mainly due to the compound reaction mechanism. In addition, the estimated fraction of compound reaction in the total cross section was found to decrease as a function of bombarding energy and neutron number of the iron isotopes. The deduced level densities for ^{55}Co, ^{55}Fe, ^{52}Mn, ^{57}Co, ^{57}Fe, and ^{54}Mn were reproduced with the Gilbert-Cameron model with parameter systematics according to Ref. [1]. Experimental data points are more consistent with the constant temperature level density behavior rather than the Fermi-gas model. The problem of the constant temperature versus Fermi-gas model is confirmed to be important for further studies of level densities and should be addressed theoretically. Understanding this feature would be important for nuclear structure physics and for reaction cross-section calculations in different applications.

The growing discrepancy between experimental and calculated cross sections for compound proton and α-particle emission was found with increasing the neutron number of iron isotopes. The most prominent discrepancy was for the d + ^{58}Fe reaction. Based on this finding, it appears very important to study how the balance between different channels in compound reactions depends on excess of neutrons (N-Z) for a particular element. This would be important to understand reactions off stability line including the rapid neutron capture reactions (r-process) in nuclear astrophysics.

VII. ACKNOWLEDGMENTS

This work was supported in part by the U.S. Department of Energy under grant numbers DE-FG02-88ER40387, DE-FG52-09NA29455, and DE-NA0001837. We would like to thank A. L. Richard and D. C. Ingram for their assistance in determining the thickness of the targets. We also acknowledge D. E. Carter, D. K. Jacobs, and J. E. O'Donnell for the technical help during the experiments in the Edwards Accelerator Laboratory.

[1] A. S. Iljinov and M. V. Mebel, Nucl. Phys. A543, 517 (1992).
[2] L. Wolfenstein, Phys. Rev. 82, 690 (1951).
W. Hauser and H. Feshbach, Phys. Rev. 87, 366 (1952).
[3] H. A. Bethe, Phys. Rev. 50, 332 (1936).
[4] R. Capote, M. Herman, P. Oblozinsky, P.G. Young, S. Goriely, T. Belgya, A.V. Ignatyuk, A.J. Koning, S. Hilaire, V.A. Plujko, M. Avrigeanu, O. Bersillon, M.B. Chadwick, T. Fukahori, Zhigang Ge, Yinlu Han, S. Kailas, J. Kopecky, V.M. Maslov, G. Reffo, M. Sin, E.Sh. Soukhovitskii and P. Talou, Nuclear Data Sheets 110, 12 (2009).
[5] S. F. Mughabghab, *Atlas of neutron resonances:resonance parameters and thermal cross sections Z=1-100*, Elsevier, Amsterdam (2006).
[6] H. Vonach, Proceedings of the IAEA Advisory Group Meeting on Basic and Applied Problems of Nuclear Level Densities, Upton NY, 1983, BNL Report No. BNL-NCS-51694, 1983, p. 247.
[7] A. V. Voinov, S. M. Grimes, C. R. Brune, M. J. Hornish, T. N. Massey, and A. Salas, Phys. Rev. C 76, 044602 (2007).
[8] R. W. Finlay, C. E. Brient, D. E. Carter, A. Marcinkowski, S. Mellema, G. Randers-Pehrson and J. Rapaport, Nucl. Instrum. Methods 198, 197 (1982).
[9] T. N. Massey, S. Al-Quraishi, C. E. Brient, J. F. Guillemette, S. M. Grimes, D. Jacobs, J. E. O Donnell, J. Oldendick, and R. Wheeler, Nucl. Sci. Eng. 129, 175

(1998).
[10] E. Simeckova, P. Bem, M. Honusek, M. Stefanik, U. Fischer, S. P. Simakov, R. A. Forrest, A. J. Koning, J. C. Sublet, M. Avrigeanu, F. L. Roman and V. Avrigeanu, Phys. Rev. C 84, 014605 (2011).
[11] M. Avrigeanu, V. Avrigeanu, P. Bem, U. Fischer, M. Honusek, K. Katovsky, C. Manailescu, J. Mrazek, E. Simeckova, and L. Zavorka, Phys. Rev. C 89, 044613 (2014).
[12] J. M. Lohr and W. Haeberli, Nucl. Phys. A 232, 381 (1974).
[13] J. Bojowald, H. Machner, H. Nann, W. Oelert, M. Rogge and P. Turek, Phys. Rev. C 38, 1153 (1988).
[14] H. An and C. Cai, Phys. Rev. C 73, 054605 (2006).
[15] S. I. Al-Quraishi, C. E. Brient, S. M. Grimes, T. N. Massey, J. Oldendick, and R. Wheeler, Phys. Rev. C62, 044616 (2000).
[16] A. J. Koning and J. P. Delaroche, Nucl. Phys. A713, 231 (2003).
[17] L. McFadden and G. R. Satchler, Nucl. Phys. 84, 177 (1966).
[18] S. M. Grimes, J. D. Anderson, J. W. McClure, B. A. Pohl, and C. Wong, Phys. Rev. C 10, 2373 (1974).
[19] C. Kalbach, Phys. Rev. 37, 2350 (1988).
[20] V. Mishra, N. Boukharouba, C. E. Brient, S. M. Grimes, and R. S. Pedroni, Phys. Rev. C 49, 750 (1994).
[21] M. Herman, R. Capote, B. V. Carlson, P. Oblozinsky, M. Sin, A. Trkov, H. Wienke, V. Zerkin, ËMPIRE: Nuclear Reaction Model Code System for Data Evaluation, Nucl. Data Sheets, 108 (2007) 2655-2715.
[22] A. Gilbert and A. G. W. Cameron, Can J. Phys. 43, 1446(1965).
[23] S. Goriely, S. Hilaire, and A. J. Koning, Phys. Rev. C 78, 064307 (2008).
[24] T. von Egidy and D. Bucurescu, Phys. Rev. C 72, 044311 (2005).
[25] T. Ericson, Nucl. Phys. A 11, 481 (1959).
[26] A. V. Ignatyuk, G. N. Smirenkin, and A. S. Tishin, Sov. J. Nucl. Phys. 21, 255 (1975).
[27] B. V. Zhuralev, A. A. Lychagin, N. N. Titarenko, V. G. Demenkov, and V. I. Trykova, Physics of Atomic Nuclei 74, 3 (2011).
[28] A. Schiller, E. Algin, L. A. Bernstein, P. E. Garrett, M. Guttormsen, M. Hjorth-Jensen, C. W. Johnson, G. E. Mitchell, J. Rekstad, S. Siem, A. Voinov and W. Younes, Phys. Rev. C 68, 054326 (2003).
[29] A. V. Voinov, B. M. Oginni, S. M. Grimes, C. R. Brune, M. Guttormsen, A. C. Larsen, T. N. Massey, A. Schiller, and S. Siem , Phys. Rev. C 79, 031301 (2009).
[30] M.Guttormsen, B.Jurado, J.N.Wilson, M.Aiche, L.A.Bernstein, Q.Ducasse, F.Giacoppo, A.Gorgen, F.Gunsing, T.W.Hagen, A.C.Larsen, M.Lebois, B.Leniau, T.Renstrom, S.J.Rose, S.Siem, T.Tornyi, G.M.Tveten, and M.Wiedeking, Phys. Rev. C 88, 024307 (2013).